



## 3D-QSAR studies of heterocyclic quinones with inhibitory activity on vascular smooth muscle cell proliferation using pharmacophore-based alignment

Chung-Kyu Ryu\*, Yoonji Lee, Seul-gi Park, Hea-Jung You, Ra-Young Lee, Seung-Yon Lee, Sun Choi\*

College of Pharmacy and Division of Life & Pharmaceutical Sciences, Ewha Womans University, Seoul 120-750, Republic of Korea

### ARTICLE INFO

#### Article history:

Received 22 July 2008

Revised 26 September 2008

Accepted 26 September 2008

Available online 30 September 2008

#### Keywords:

Antiproliferative

Vascular smooth muscle cell

QSAR

CoMFA

CoMSIA

Quinoxaline-5,8-dione

1H-benzo[d]imidazole-4,7-dione

### ABSTRACT

The abnormal proliferation and migration of vascular smooth muscle cells (SMCs) play an important role in the pathology of coronary artery atherosclerosis and restenosis following angioplasty. It was reported that some heterocyclic quinone derivatives such as 6-aryl-amino-quinoxaline-5,8-diones and 6-aryl-amino-1H-benzo[d]imidazole-4,7-diones have inhibitory activity on rat aortic smooth muscle cell (RAoSMC) proliferation. To understand the structural basis for antiproliferative activity to design more potent agents, we generated pharmacophore models of representative molecules with high activity using Genetic Algorithm with Linear Assignment of Hypermolecular Alignment of Database (GALAHAD) and aligned a series of compounds to the selected pharmacophore model, then performed three-dimensional quantitative structure–activity relationship (3D-QSAR) studies using Comparative Molecular Field Analysis (CoMFA) and Comparative Molecular Similarity Indices Analysis (CoMSIA).

Good cross-validated correlations were obtained with CoMFA (resulting in  $q^2$  of 0.734 and  $r^2$  of 0.947) and CoMSIA (resulting in  $q^2$  of 0.736 and  $r^2$  of 0.913). The  $IC_{50}$  values of the heterocyclic quinone derivatives on RAoSMC exhibited a strong correlation with steric and hydrophobic fields of the 3D structure of the molecules, resulting in the reliable prediction of inhibitory activity of the series of compounds.

© 2008 Elsevier Ltd. All rights reserved.

### 1. Introduction

The abnormal proliferation and migration of vascular smooth muscle cells (SMCs) play a pivotal role in progression of coronary artery atherosclerosis and restenosis following angioplasty.<sup>1</sup> Arterial injury results in the migration of SMCs into the intimal layer of the arterial wall, where they proliferate and synthesize extracellular matrix components. Heterocyclic quinonoid compounds are an attractive class of biologically active molecules.<sup>2</sup> Therefore, we synthesized and tested various quinone derivatives to elucidate their contribution to the antiproliferative effects on PDGF-stimulated SMC proliferation. Among the tested quinones, 1H-benzo[d]imidazole-4,7-dione and quinoxaline-5,8-dione derivatives **1–10** showed potent antiproliferative activity (Fig. 1).

It was reported that some quinonoid derivatives such as 1H-benzo[d]imidazole-4,7-diones **1–4**,<sup>3,4</sup> **6–8**,<sup>5</sup> and quinoxaline-5,8-diones **9**<sup>6</sup> have their antiproliferative activity on rat aortic smooth muscle cells. We newly synthesized quinoxaline-5,8-diones **10** and tested them to elucidate their contribution to the antiproliferative effects on PDGF-stimulated SMC proliferation. Also, 6-aryl-amino-

2-(2-pyridyl)-1H-benzo[d]imidazole-4,7-diones **5**<sup>7</sup> were evaluated in vitro for their antiproliferative activity on the SMCs.

To understand the structural basis for antiproliferative activity to design more potent agents, we performed three-dimensional quantitative structure–activity relationship (3D-QSAR) studies for a series of compounds using Comparative Molecular Field Analysis (CoMFA) and Comparative Molecular Similarity Indices Analysis (CoMSIA). First, we generated pharmacophore model of representative molecules with high activity using Genetic Algorithm with Linear Assignment of Hypermolecular Alignment of Database (GALAHAD) and aligned all the molecules to the model. Then, 3D-QSAR analyses were performed. The antiproliferative activities of heterocyclic quinone derivatives on rat aortic smooth muscle cell (RAoSMC) exhibited a strong relationship with the molecular interaction fields from the 3D-QSAR studies, resulting in reliable prediction of inhibitory activity of a series of compounds.

### 2. Chemistry and biological activities

The  $IC_{50}$  values of compounds, 6-aryl-amino-1H-benzo[d]imidazole-4,7-diones **1–4**,<sup>3,4</sup> 6-aryl-amino-2-(2-pyridyl)-1H-benzo[d]imidazole-4,7-diones **5**, 6-aryl-amino-5-chloro-2-(2-pyridyl)-1H-benzo[d]imidazole-4,7-diones **6–8**,<sup>5</sup> 6-aryl-amino-2,3-bis(pyridin-2-yl)-7-chloro-quinoxaline-5,8-diones **9**,<sup>6</sup> and 6-aryl-amino-2,3-bis(methyl)-quinoxaline-5,8-diones **10** were used for this analysis

\* Corresponding authors. Tel.: +82 2 3277 3027; fax: +82 2 3277 3051 (C.-K.R.); tel.: +82 2 3277 4503; fax: +82 2 3277 2851 (S.C.).

E-mail addresses: [ckryu@mm.ewha.ac.kr](mailto:ckryu@mm.ewha.ac.kr) (C.-K. Ryu), [sunchoi@ewha.ac.kr](mailto:sunchoi@ewha.ac.kr) (S. Choi).

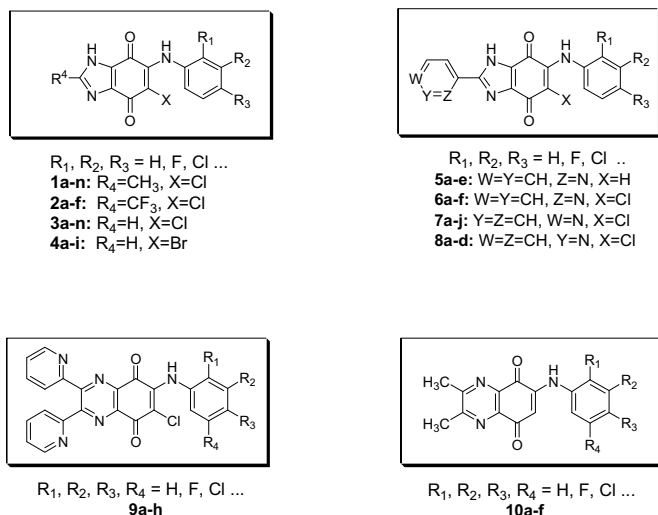


**Figure 1.** Quinoxaline-5,8-dione and 1H-benzo[d]imidazole-4,7-dione derivatives.

(Tables 1 and 2). Among them, compounds **10** were newly synthesized and tested to elucidate their contribution to the antiproliferative effects on PDGF-stimulated SMC proliferation. The method used to synthesize the quinoxaline-5,8-diones **10a–f** is shown in Scheme 1. 2,3-bis(Methyl)-5,8-hydroxyquinoxaline (**11**) was prepared

according to the known method<sup>8</sup> with minor modifications. 2,3-Bis(-methyl)-quinoxaline-5,8-dione (**12**) was synthesized by oxidizing compound **11** with  $Ag_2O$  in 79% yields. 6-Arylamino-2,3-bis(-methyl)-quinoxaline-5,8-diones **10a–f** were prepared by substitution on compound **12** with appropriate arylamines. Most of these substitutions went as expected.

The compounds **5a–e** were prepared by nucleophilic substitution on each 2-(2-pyridyl)-4,7-1H-benzo[d]imidazole-4,7-dione **13** with arylamines according to the reported method<sup>7</sup> to evaluate the antiproliferative effects on PDGF-stimulated SMC proliferation.

The newly prepared compounds **5a–e** and **10a–f** were evaluated in vitro for their antiproliferative activity on the RAoSMCs. Inhibition of proliferation of these cells was determined by published assay method<sup>6</sup> and the  $IC_{50}$  values were determined and compared to the positive control mycophenolic acid (MPA). Their structures and activities are summarized in Tables 1 and 2.

### 3. 3D-QSAR modeling

The training (65 compounds) and test sets (17 compounds) used in these studies comprise a series of the 6-phenylamino-1H-benzo[d]imidazole-4,7-diones and 6-phenylamino-quinoxaline-5,8-diones. The  $IC_{50}$  values were converted to  $pIC_{50}$  (i.e.,  $-\log IC_{50}$ ) and used as dependent variables in CoMFA and CoMSIA QSAR analyses. The distribution of biological activities of training set and test set versus % of compounds is shown in Figure 2.

**Table 1**

Structures and  $IC_{50}$  values of the 6-phenylamino-1H-benzo[d]imidazole-4,7-diones for inhibition of SMC proliferation

Compound	X	R <sub>1</sub>	R <sub>2</sub>	R <sub>3</sub>	R <sub>4</sub>	$IC_{50}^b$ (μM)	Compound	X	R <sub>1</sub>	R <sub>2</sub>	R <sub>3</sub>	R <sub>4</sub>	$IC_{50}^b$ (μM)
<b>1a</b> <sup>3</sup>	Cl	H	H	H	CH <sub>3</sub>	0.8	<b>4a</b> <sup>4</sup>	Br	H	H	H	H	1.1
<b>1b</b> <sup>4</sup>	Cl	H	H	F	CH <sub>3</sub>	3.0	<b>4b</b> <sup>a,4</sup>	Br	H	H	F	H	1.0
<b>1c</b> <sup>a,4</sup>	Cl	H	H	Cl	CH <sub>3</sub>	2.8	<b>4c</b> <sup>4</sup>	Br	H	H	Cl	H	4.0
<b>1d</b> <sup>3</sup>	Cl	H	H	I	CH <sub>3</sub>	1.0	<b>4d</b> <sup>3</sup>	Br	H	H	CH <sub>3</sub>	H	1.0
<b>1e</b> <sup>3</sup>	Cl	H	H	CH <sub>3</sub>	CH <sub>3</sub>	0.8	<b>4e</b> <sup>3</sup>	Br	H	H	CF <sub>3</sub>	H	3.1
<b>1f</b> <sup>a,4</sup>	Cl	H	H	CH <sub>2</sub> CH <sub>3</sub>	CH <sub>3</sub>	3.0	<b>4f</b>	Br	H	Cl	H	H	3.0
<b>1g</b> <sup>4</sup>	Cl	H	H	CF <sub>3</sub>	CH <sub>3</sub>	0.6	<b>4g</b> <sup>4</sup>	Br	H	Br	H	H	5.3
<b>1h</b> <sup>4</sup>	Cl	H	H	OCF <sub>3</sub>	CH <sub>3</sub>	3.0	<b>4h</b> <sup>4</sup>	Br	H	I	H	H	2.5
<b>1i</b> <sup>4</sup>	Cl	H	Cl	H	CH <sub>3</sub>	0.9	<b>4i</b> <sup>4</sup>	Br	H	CF <sub>3</sub>	H	H	3.0
<b>1j</b> <sup>3</sup>	Cl	H	Br	H	CH <sub>3</sub>	1.0	<b>5a</b> <sup>5</sup>	H	H	H	Cl	<i>o</i> -Pyridine	13
<b>1k</b> <sup>4</sup>	Cl	F	H	F	CH <sub>3</sub>	1.2	<b>5b</b> <sup>5</sup>	H	H	H	Br	<i>o</i> -Pyridine	12
<b>1l</b> <sup>3</sup>	Cl	Cl	H	Cl	CH <sub>3</sub>	0.8	<b>5c</b> <sup>5</sup>	H	H	H	I	<i>o</i> -Pyridine	20
<b>1m</b> <sup>4</sup>	Cl	Cl	Cl	H	CH <sub>3</sub>	0.6	<b>5d</b> <sup>5</sup>	H	H	H	OCH <sub>2</sub> CH <sub>3</sub>	<i>o</i> -Pyridine	6.5
<b>1n</b> <sup>4</sup>	Cl	F	F	F	CH <sub>3</sub>	0.8	<b>5e</b> <sup>5</sup>	H	H	H	OCF <sub>3</sub>	<i>o</i> -Pyridine	20
<b>2a</b> <sup>3</sup>	Cl	H	H	H	CF <sub>3</sub>	50.0	<b>6a</b> <sup>5</sup>	Cl	H	H	Cl	<i>o</i> -Pyridine	12
<b>2b</b> <sup>3</sup>	Cl	H	H	F	CF <sub>3</sub>	12.0	<b>6b</b> <sup>5</sup>	Cl	H	H	Br	<i>o</i> -Pyridine	6.5
<b>2c</b> <sup>a,3</sup>	Cl	H	H	Cl	CF <sub>3</sub>	15.0	<b>6c</b> <sup>5</sup>	Cl	H	H	OCF <sub>3</sub>	<i>o</i> -Pyridine	6
<b>2d</b> <sup>3</sup>	Cl	H	H	I	CF <sub>3</sub>	25.0	<b>6d</b> <sup>5</sup>	Cl	H	Cl	H	<i>o</i> -Pyridine	3.5
<b>2e</b> <sup>3</sup>	Cl	H	H	CH <sub>3</sub>	CF <sub>3</sub>	40.0	<b>6e</b> <sup>5</sup>	Cl	H	Br	H	<i>o</i> -Pyridine	20
<b>2f</b> <sup>3</sup>	Cl	H	H	CF <sub>3</sub>	CF <sub>3</sub>	20.0	<b>6f</b>	Cl	F	H	H	<i>o</i> -Pyridine	9.4
<b>3a</b> <sup>a,3</sup>	Cl	H	H	H	H	5.5	<b>7a</b> <sup>5</sup>	Cl	H	H	F	<i>p</i> -Pyridine	50
<b>3b</b> <sup>4</sup>	Cl	H	H	F	H	1.2	<b>7b</b> <sup>5</sup>	Cl	H	H	Br	<i>p</i> -Pyridine	60
<b>3c</b> <sup>4</sup>	Cl	H	H	Br	H	2.0	<b>7c</b> <sup>a,5</sup>	Cl	H	H	OCH <sub>3</sub>	<i>p</i> -Pyridine	50
<b>3d</b> <sup>a,3</sup>	Cl	H	H	I	H	1.3	<b>7d</b> <sup>5</sup>	Cl	H	H	OCH <sub>2</sub> CH <sub>3</sub>	<i>p</i> -Pyridine	75
<b>3e</b> <sup>3</sup>	Cl	H	H	CH <sub>3</sub>	H	1.4	<b>7e</b> <sup>5</sup>	Cl	H	F	H	<i>p</i> -Pyridine	19
<b>3f</b> <sup>a,3</sup>	Cl	H	H	CF <sub>3</sub>	H	2.5	<b>7f</b>	Cl	H	Cl	H	<i>p</i> -Pyridine	31
<b>3g</b> <sup>4</sup>	Cl	H	H	OCF <sub>3</sub>	H	2.5	<b>7g</b> <sup>a,5</sup>	Cl	H	Br	H	<i>p</i> -Pyridine	20
<b>3h</b> <sup>4</sup>	Cl	H	H	CN	H	2.7	<b>7h</b> <sup>5</sup>	Cl	H	CH <sub>3</sub>	H	<i>p</i> -Pyridine	60
<b>3i</b> <sup>4</sup>	Cl	H	Cl	H	H	1.4	<b>7i</b> <sup>a,5</sup>	Cl	H	F	Cl	<i>p</i> -Pyridine	25
<b>3j</b> <sup>3</sup>	Cl	H	Br	H	H	1.6	<b>7j</b> <sup>5</sup>	Cl	H	Cl	Cl	<i>p</i> -Pyridine	13
<b>3k</b> <sup>3</sup>	Cl	H	I	H	H	1.3	<b>8a</b> <sup>5</sup>	Cl	H	H	F	<i>m</i> -Pyridine	21
<b>3l</b> <sup>4</sup>	Cl	H	F	F	H	1.1	<b>8b</b> <sup>5</sup>	Cl	H	H	Cl	<i>m</i> -Pyridine	20
<b>3m</b> <sup>a,4</sup>	Cl	F	H	H	H	1.7	<b>8c</b> <sup>a,5</sup>	Cl	H	H	CeHo	<i>m</i> -Pyridine	45
<b>3n</b> <sup>4</sup>	Cl	F	H	F	H	2.7	<b>8d</b> <sup>5</sup>	Cl	H	H	OCH <sub>2</sub> CH <sub>3</sub>	<i>m</i> -Pyridine	42

<sup>a</sup> Compounds in test set.

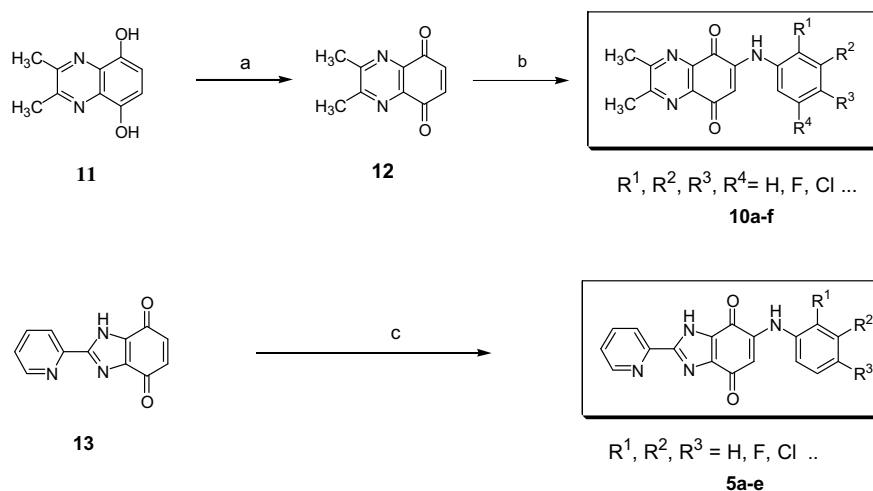
<sup>b</sup> The inhibitory activity against the PDGF-induced proliferation of the SMCs isolated from rat thoracic aorta.

**Table 2**  
Structures and IC<sub>50</sub> values of the 6-phenylamino-quinoxaline-5,8-diones for inhibition of SMC proliferation

Compound	X	R <sub>1</sub>	R <sub>2</sub>	R <sub>3</sub>	R <sub>4</sub>	R <sub>5</sub>	R <sub>6</sub>	IC <sub>50</sub> <sup>b</sup> (μM)
<b>9a</b> <sup>6</sup>	Cl	H	H	H	H	<i>o</i> -Pyridine	<i>o</i> -Pyridine	3.1
<b>9b</b> <sup>6</sup>	Cl	H	H	F	H	<i>o</i> -Pyridine	<i>o</i> -Pyridine	1.0
<b>9c</b> <sup>a,6</sup>	Cl	H	H	Cl	H	<i>o</i> -Pyridine	<i>o</i> -Pyridine	1.5
<b>9d</b> <sup>a,6</sup>	Cl	H	H	OH	H	<i>o</i> -Pyridine	<i>o</i> -Pyridine	5.5
<b>9e</b> <sup>a,6</sup>	Cl	H	H	OCH <sub>3</sub>	H	<i>o</i> -Pyridine	<i>o</i> -Pyridine	3.5
<b>9f</b> <sup>6</sup>	Cl	H	H	OCF <sub>3</sub>	H	<i>o</i> -Pyridine	<i>o</i> -Pyridine	1.0
<b>9g</b> <sup>6</sup>	Cl	H	Cl	Cl	H	<i>o</i> -Pyridine	<i>o</i> -Pyridine	1.0
<b>9h</b> <sup>6</sup>	Cl	H	F	F	F	<i>o</i> -Pyridine	<i>o</i> -Pyridine	1.2
<b>10a</b> <sup>a</sup>	H	H	H	F	H	CH <sub>3</sub>	CH <sub>3</sub>	3.1
<b>10b</b>	H	H	H	Cl	H	CH <sub>3</sub>	CH <sub>3</sub>	3.3
<b>10c</b>	H	H	H	Br	H	CH <sub>3</sub>	CH <sub>3</sub>	1.1
<b>10d</b>	H	H	H	OCH <sub>2</sub> CH <sub>3</sub>	H	CH <sub>3</sub>	CH <sub>3</sub>	1.5
<b>10e</b>	H	H	F	F	F	CH <sub>3</sub>	CH <sub>3</sub>	4.5
<b>10f</b>	H	H	Cl	Cl	H	CH <sub>3</sub>	CH <sub>3</sub>	3.8

<sup>a</sup> Compounds in test set.

<sup>b</sup> The inhibitory activity against the PDGF-induced proliferation of the SMCs isolated from rat thoracic aorta.



**Scheme 1.** Synthesis of 6-aryl-amino-2,3-bis(methyl)-quinoxaline-5,8-diones and 2-aryl-6-aryl-amino-1H-benzo[d]imidazole-4,7-diones. Reagents and conditions: (a) Ag<sub>2</sub>O/rt/4 h/79%; (b) arylamine (1 equiv)/EtOH/reflux/10 h/31–53%; (c) arylamine (1 equiv)/EtOH/reflux/5 h/66–84%.

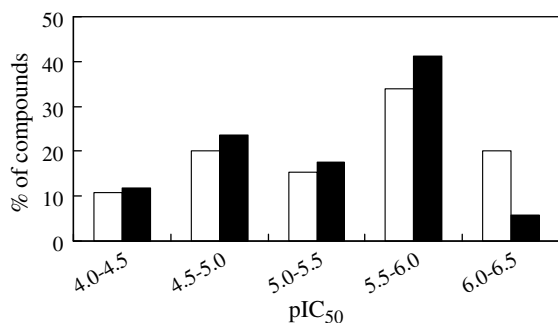


**Figure 2.** Distribution of biological activities for training set and test set versus % of compounds. (White bars: training set; black bars: test set.)

Since the major weakness of the traditional 3D-QSAR has been the alignment of the molecules, we applied pharmacophore modeling using GALAHAD in order to get the more reasonable alignment results. First, the representative molecules with high activities were selected among the training set. Then, pharmacophore models were generated using the selected molecules (i.e.,

**1m, 1n, 1g, 5d, 6d, 9g, and 10c**), and all the other molecules were aligned to the best pharmacophore model. The alignment of the molecules is shown in Figure 3.

Two different 3D-QSAR methods, CoMFA and CoMSIA were applied to find a correlation between molecular property fields of the aligned molecules and their activities. Leave-one-out (LOO) cross-validated PLS analyses were performed to determine the optimal number of components to be used in the final QSAR models and to check the predictive ability of the models. The resulting contour maps from the CoMFA and CoMSIA models showed the steric, hydrophobic, and hydrogen-bond acceptor requirements of the series of compounds for inhibitory activity and these findings would be used for designing more potent inhibitors against SMC proliferation.

## 4. Results and discussion

### 4.1. CoMFA and CoMSIA statistical results

The statistical results for 3D-QSAR modeling are summarized in Table 3. PLS analyses gave cross-validated  $q^2$  of 0.734 for CoMFA,

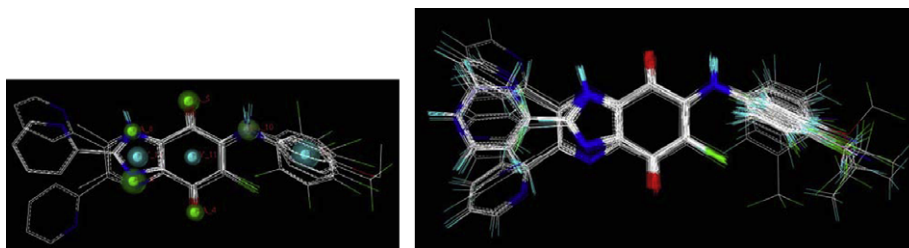


**Figure 3.** Selected pharmacophore model and molecular alignments using that model. Cyan and green spheres are represented for hydrophobes and hydrogen-bond acceptors, respectively.

**Table 3**  
Summary of CoMFA and CoMSIA results

	CoMFA	CoMSIA
$q^2_{\text{a}}$	0.734	0.736
$r^2_{\text{b}}$	0.947	0.913
SEE <sup>c</sup>	0.147	0.189
F value	174.153	101.639
$r^2_{\text{pred}}^{\text{d}}$	0.814	0.793
No. of compounds	65	65
NOC <sup>e</sup>	6	6
<b>Contribution</b>		
Steric	0.586	0.130
Electrostatic	0.414	0.447
Hydrophobic	—	0.233
H-bond donor	—	0.060
H-bond acceptor	—	0.130

<sup>a</sup> Cross-validated correlation coefficient after leave-one-out procedure.

<sup>b</sup> Correlation coefficient.

<sup>c</sup> Standard error of estimate.

<sup>d</sup> Predicted correlation coefficient for test set of compounds.

<sup>e</sup> Optimal number of components.

and  $q^2$  of 0.736 for CoMSIA with six components in both models. Figure 4 shows the strong correlations between the actual versus predicted  $\text{pIC}_{50}$  values for 65 compounds in the training set by CoMFA and CoMSIA models. The correlation coefficients for CoMFA and CoMSIA were 0.947 and 0.913, respectively.

A set of 17 compounds, not included in the model generation, was prepared to determine the predictive abilities of the CoMFA and CoMSIA models. Both models well predicted the activities of the test set compounds. The predicted  $r^2$  values from the CoMFA and CoMSIA models were found to be 0.814 and 0.793, respectively. The comparison between the actual versus predicted  $\text{pIC}_{50}$  values for the test set based on the CoMFA and CoMSIA models are presented in Table 4 and Figure 5. These data indicate that reliable CoMFA and CoMSIA models were successfully constructed.

For comparison, we also performed 3D-QSAR studies based on atom-by-atom alignment. The resulting  $q^2$  and  $r^2$  values were similar to those of pharmacophore-alignment based QSAR studies;  $q^2 = 0.748$  and  $r^2 = 0.942$  for CoMFA,  $q^2 = 0.743$  and  $r^2 = 0.907$  for CoMSIA. But in this case, the predictability of the test set (i.e.,  $r^2_{\text{pred}}$ ) was decreased to 0.704 for CoMFA and 0.700 for CoMSIA.

Although atom-by-atom alignment would result in more perfect fit in a congeneric series of compounds, whether that alignment represents what is happening inside the biological system would be questionable. As shown in some reported co-crystallized structures of a congeneric series of compounds, the alignment of active conformers do not necessarily display perfect match as shown in atom-by-atom alignment. That might be because each compound would change its conformation, even in congeneric part, to achieve the best activity in the biological system. Therefore, using pharmacophore-based alignment could be a reasonable way for more realistic 3D-QSAR studies when the active conformations of tested compounds are not available as in crystal structures.

## 4.2. CoMFA contour maps

According to the 3D-QSAR results, the contour maps were created using the data from PLS analyses. These maps help us to explain the chemical property features of the compounds which influence the biological activities.

Figure 6(a) and (b) shows the steric and electrostatic maps for the CoMFA model on compounds **1g** and **9g**, which are the most active compounds in each series, respectively. In the steric CoMFA map, the green contour indicates the areas in which steric bulk on an inhibitor is favored, and the yellow contour represents the regions in which steric bulk is disfavored to overall inhibitory activity. The electrostatic contour maps are shown as red and blue contours in Figure 6(c) and (d). The red contour means the regions in which the electronegative groups in the ligands are associated with increased antiproliferative activities, while the blue contour

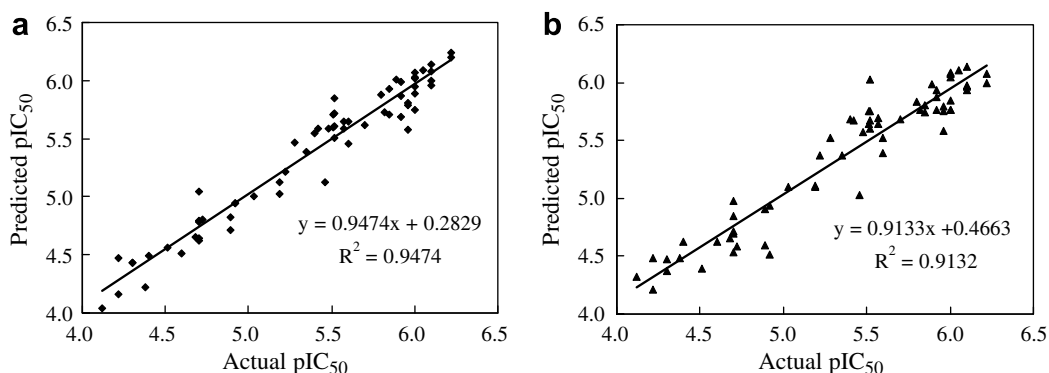


**Figure 4.** Plots of predicted versus actual  $\text{pIC}_{50}$  values for the training set molecules based on (a) CoMFA and (b) CoMSIA models.

**Table 4**  
Observed and predicted activities for the test set by CoMFA and CoMSIA models

Compound	pIC <sub>50</sub>	CoMFA		CoMSIA	
		Predict	Residual	Predict	Residual
1c <sup>4</sup>	5.55	5.913	-0.36	5.945	-0.39
1f <sup>4</sup>	5.52	5.993	-0.47	6.068	-0.55
2c <sup>3</sup>	4.82	4.749	0.07	4.521	0.30
3a <sup>3</sup>	5.26	5.676	-0.42	5.648	-0.39
3d <sup>3</sup>	5.89	5.616	0.27	5.776	0.11
3f <sup>3</sup>	5.60	5.629	-0.03	5.627	-0.03
3m <sup>4</sup>	5.77	5.609	0.16	5.692	0.08
4b <sup>4</sup>	6.00	5.588	0.41	5.778	0.22
6f <sup>5</sup>	4.92	4.938	-0.02	5.014	-0.09
7c <sup>5</sup>	4.30	4.164	0.14	4.463	-0.16
7g <sup>5</sup>	4.70	4.554	0.15	4.289	0.41
7i <sup>5</sup>	4.60	4.654	-0.05	4.571	0.03
8c <sup>5</sup>	4.35	4.630	-0.28	4.651	-0.30
9c <sup>6</sup>	5.82	5.817	0.00	5.750	0.07
9d <sup>6</sup>	5.26	5.229	0.03	4.964	0.30
9e <sup>6</sup>	5.46	5.693	-0.23	5.738	-0.28
10a	5.51	5.609	-0.10	5.604	-0.09

displays the areas that positively charged groups have improved biological activity and thus lower the IC<sub>50</sub> values.

According to the CoMFA contour maps, the sterically bulky groups on R<sub>4</sub> position of the 6-phenylamino-1H-benzo[d]imidazole-4,7-dione series would be detrimental to activity. On the other

hand, R<sub>5</sub> position of the 6-phenylamino-quinoxaline-5,8-dione series may be favorable in bulky groups. As in the case of compounds **5a–d**, **6a–f**, **7a–i**, and **8a–d**, the substitution of bulky pyridine ring on the R<sub>4</sub> position decreases the overall biological activity. On the other hand, in case of compound **9a–9h**, the substitution of pyridine ring on R<sub>5</sub> position does not negatively affect their activities.

### 4.3. CoMSIA contour maps

The steric and electrostatic maps of CoMSIA are quite similar to those of CoMFA. Figure 7(a) and (b) show the steric maps for CoMSIA model for compounds **1g** and **9g**, respectively. According to CoMSIA steric fields, the sterically bulky groups on R<sub>4</sub> position of the 6-phenylamino-1H-benzo[d]imidazole-4,7-dione series have a negative effect on the activity, as shown in the CoMFA steric map. On the other hand, R<sub>5</sub> and R<sub>6</sub> position of the 6-phenylamino-quinoxaline-5,8-dione series may be favorable in bulky groups.

The hydrogen-bond acceptor map of the CoMSIA model on compound **9g** is presented in Figure 7(e). The magenta and green-blue indicate the areas occupied by hydrogen-bond acceptor groups exerting favorable and unfavorable effects on SMC antiproliferation, respectively. A large magenta polyhedron, around the R<sub>4</sub> position of the 6-phenylamino-1H-benzo[d]imidazole-4,7-dione series and R<sub>5</sub> or R<sub>6</sub> positions of the 6-phenylamino-quinoxaline-5,8-dione series, indicates the location of hydrogen-bond acceptor groups having an enhancing effect on SMC antiproliferation. This result

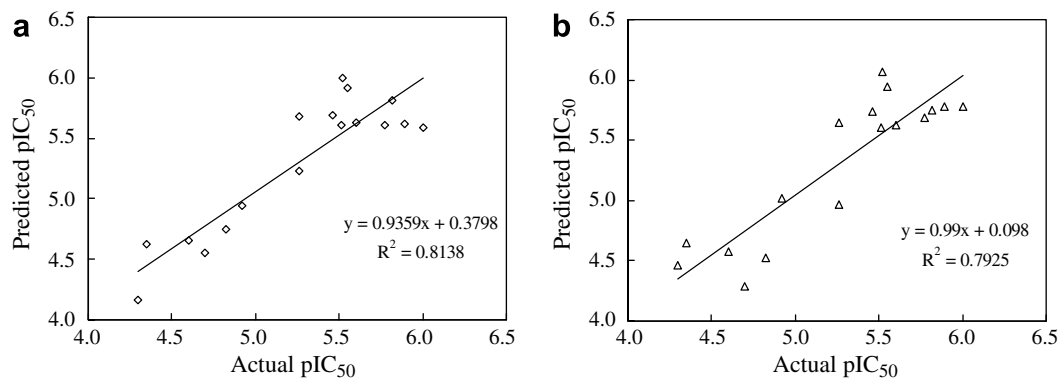


**Figure 5.** Plots of predicted versus actual pIC<sub>50</sub> values for the test set molecules based on (a) CoMFA and (b) CoMSIA models.

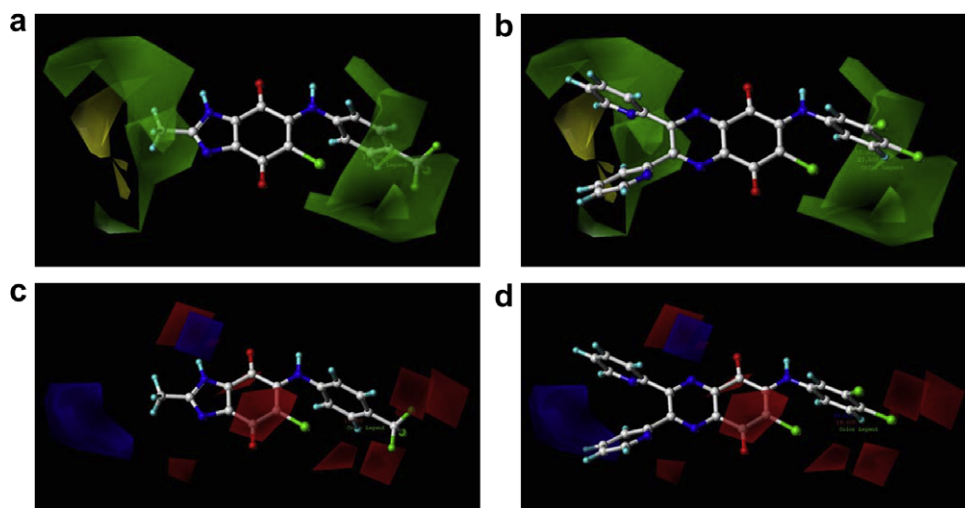


**Figure 6.** CoMFA contour maps for steric and electrostatic fields. (a) Steric map displayed with compound **1g**; (b) steric map with compound **9g**; (c) electrostatic map with compound **1g**; (d) electrostatic map with compound **9g**. Sterics: green (favored)/yellow (disfavored); electrostatics: blue (positive-charge favored)/red (negative-charge favored).

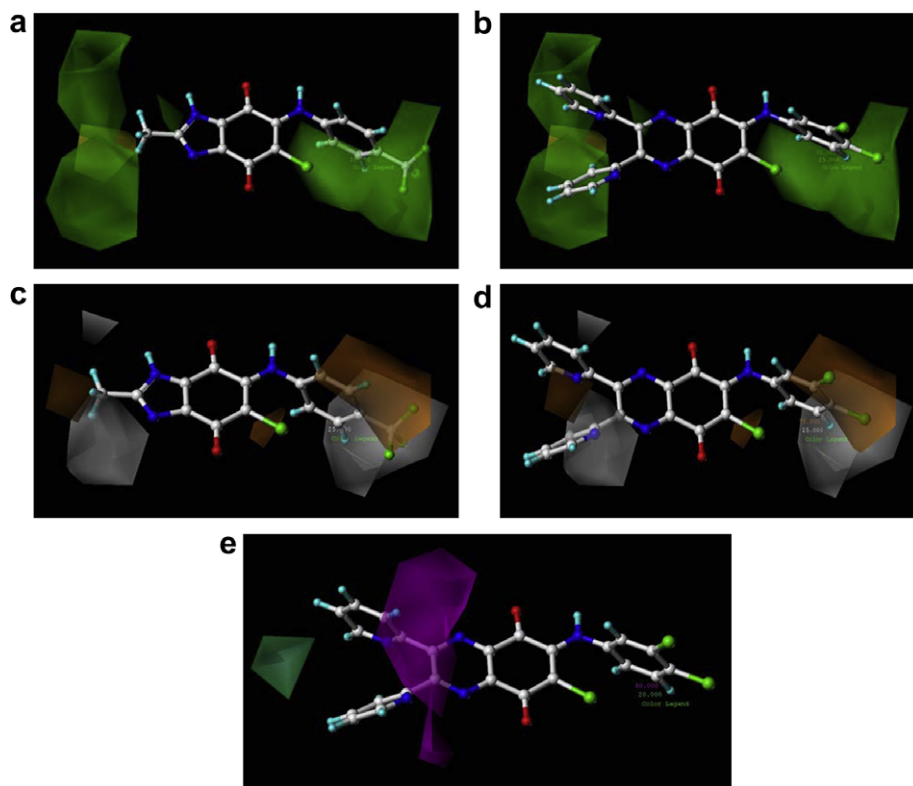


**Figure 7.** CoMSIA contour maps for steric, hydrophobic and H-bond acceptor fields. (a) Steric map displayed with compound **1g**; (b) steric map with compound **9g**; (c) hydrophobic map with compound **1g**; (d) hydrophobic map with compound **9g**; (e) H-bond acceptor map with compound **9g**. Sterics: green (favored)/yellow (disfavored); hydrophobic: brown (favored)/white (disfavored); hydrogen bonding acceptor: magenta (favored)/green-blue (disfavored).

is consistent with the fact that compounds with *o*-pyridine substituent in those positions showed much better activities than those with *m*- or *p*-pyridine.

The hydrophobic maps of the CoMSIA model on compounds **1g** and **9g** are shown in Figure 7(c) and (d), respectively. The brown and white represents the areas where hydrophobic properties are favored and disfavored, respectively.  $R_4$  position of the 6-phenylamino-1H-benzo[d]imidazole-4,7-dione series is hydrophobic-favored region, thus the compounds substituted with the hydrophobic groups on that position were more potent than unsubstituted compounds. The hydrophobic-favored region in  $R_4$  position coincided with the fact that the methyl-substituted compound **1** series was more active than non-substituted compounds. Although trifluoromethyl group is more hydrophobic than methyl group, it is an electron-withdrawing group and that might negatively contribute to the biological activity.

To compare the deviation of electron density (of  $\text{CF}_3$ - and  $\text{CH}_3$ -containing compounds), we calculated their atomic charges by Gasteiger–Hückel method. We found that the electron density of the whole molecule changed when it was substituted with  $\text{CF}_3$  in  $R_4$  position. As Figure 8 shows, electron density in the quinone ring decreased after substituted with  $\text{CF}_3$  in compound **2a**. The quinone ring is thought to be critical to the biological activity, and the changes of its electron density might have caused the decrease of the activity.

According to the electrostatic contour map (Fig. 6(c) and (d)), the quinone ring is (–)-charge favored region for better activity. It is consistent with the result that compound **2a** (with the electron-withdrawing  $\text{CF}_3$  group) is less active compared with others. The low activity of  $\text{CF}_3$  substituted compounds may also be influenced by the decrease of H-bonding ability of hetero atoms in the quinone ring. To clarify this point, synthesis of the compounds

with electron-donating and less hydrophobic groups in  $R_4$  position is in progress.

## 5. Conclusions

A series of the 6-phenylamino-1H-benzo[d]imidazole-4,7-diones and 6-phenylamino-quinoxaline-5,8-diones were synthesized and their 3D-QSAR studies were performed, resulting in the good cross-validated correlations obtained by CoMFA ( $q^2$  of 0.734 and  $r^2$  of 0.947) and CoMSIA ( $q^2$  of 0.736 and  $r^2$  of 0.913). The predictive ability of CoMFA and CoMSIA, determined by a test set, gave good predictive correlation coefficients of 0.814 and 0.793, respectively.

The steric, hydrophobic, and hydrogen-bond acceptor requirements for the inhibitory activity are well described from the contour maps of these studies. It appears that the pharmacophore-based alignment provided reasonable superimposition of the molecules for our 3D-QSAR studies. Along with the pharmacophore model, more precise pharmacophore features were suggested by the contour maps, and these results would be further utilized to design more potent inhibitors of smooth muscle cell proliferation.

## 6. Experimental

All melting points were measured in open capillary tubes with a Büchi melting point B-545 and were uncorrected. TLC was performed on precoated silica gel (60G 254, Merck) using chloroform as a solvent. The compounds were detected under UV light (254 nm) or by heating to 110 °C after spraying with a 30%  $\text{H}_2\text{SO}_4$ -vanillin solution. Column chromatography was performed on silica gel G60 (70–230 mesh, ASTM, Merck).  $^1\text{H}$  NMR spectra were recorded on Unity Varian INOVA 400 MHz FT-NMR spectrom-

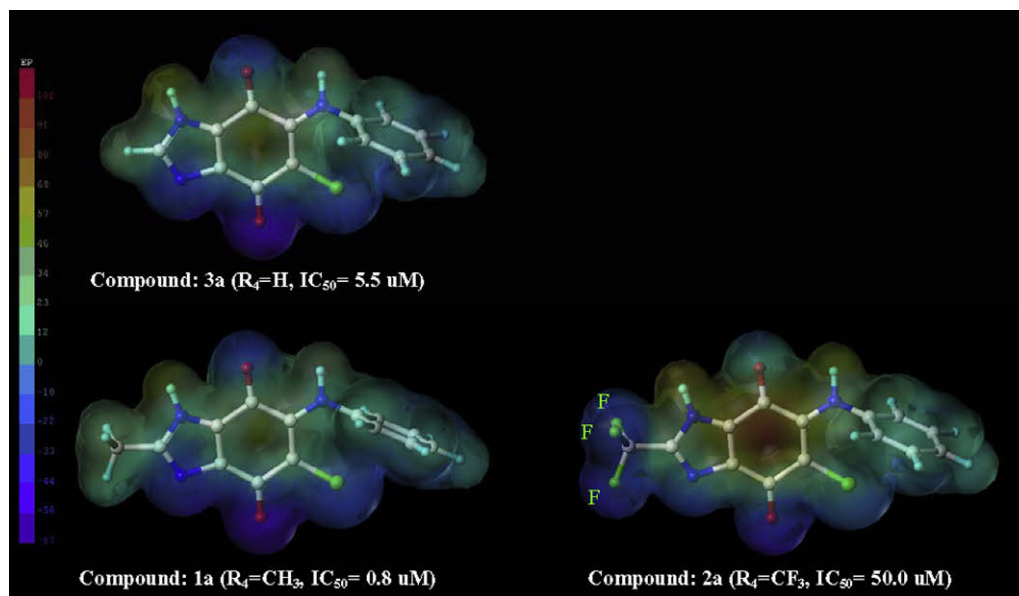


**Figure 8.** Molecular surfaces of compound **1a**, **2a**, and **3a** colored by electrostatic potential (EP). Van der Waals surfaces were generated by MOLCAD and displayed in transparent style. The electrostatic potential at each surface was computed with a global range for the property from red (most positive) to purple (most negative), so identical colors on the surfaces of different molecules reflect the identical property values.

eter using DMSO- $d_6$  as a solvent, and chemical shifts were given in ppm with TMS as a standard. High-resolution mass spectra (HRMS EI) were obtained on a Jeol JMS AX505 WA. 2,3-Bis(methyl)-5,8-hydroxy-5,8-dihydroquinoxaline (**11**) was prepared according to the known method.<sup>8</sup> Other reagents were purchased from Aldrich Chemical Co.

### 6.1. Synthesis of the 2,3-bis(methyl)-quinoxaline-5,8-dione (**12**)

Compounds **11** 1.26 g (6.6 mmol) was suspended in 500 mL of 1,2-diethoxyethane and treated  $\text{Ag}_2\text{O}$  1.9 g (7.7 mmol) for 4 h at rt in the dark. The solvent was removed under vacuum, and the crude product was purified by silica gel column chromatography with  $\text{CHCl}_3$ . Crystallization from aq. EtOH afforded compound **12**; 79%, mp 179–181 °C (lit.<sup>8</sup> mp 182 °C dec).

### 6.2. General procedure for synthesis of the 6-aryl-amino-2,3-bis(methyl)-quinoxaline-5,8-diones **10**

A solution of compound **12** 0.063 g (0.34 mmol) in 15 mL of 95% EtOH was added to the solution of the arylamine (0.35 mmol) in 5 mL of 95% EtOH and stirred at rt for 1 h and then refluxed for 10 h. After the mixture was kept overnight in the refrigerator or poured into 20 mL of ice water, the precipitate was collected by filtration. The crude product was purified by silica gel column chromatography with  $\text{CHCl}_3$  and MeOH. Crystallization from aq. EtOH afforded the compounds **10a–f**.

#### 6.2.1. 2,3-Dimethyl-6-(4-fluorophenyl)amino-5,8-quinoxalinedione (**10a**)

Dark purple powder (53%). mp: 248–249 °C  $^1\text{H NMR}$  (DMSO- $d_6$ ):  $\delta$  9.4 (s, 1H, NH), 7.2–7.4 (m, 4H, benzene), 6.0 (s, 1H, H7), 2.7 (s, 6H, 2CH<sub>3</sub>). MS ( $m/z$ ): 297 ( $\text{M}^+$ ), 282, 278, 136, 162, 96, 84, 57. HRMS ( $m/z$ ): Calcd for  $\text{C}_{16}\text{H}_{12}\text{O}_2\text{N}_3\text{F}$  297.0914 Found: 297.0914.

#### 6.2.2. 6-(4-Chlorophenyl)amino-2,3-dimethyl-5,8-quinoxalinedione (**10b**)

Dark violet powder (41%). mp: 253–254 °C  $^1\text{H NMR}$  (DMSO- $d_6$ ):  $\delta$  9.4 (s, 1H, NH), 7.4–7.5 (m, 4H, benzene), 6.2 (s, 1H, H7), 2.6 (s,

6H, CH<sub>3</sub>). MS ( $m/z$ ): 313 ( $\text{M}^+$ ), 298, 278, 236, 199, 97, 84, 57. HRMS ( $m/z$ ): Calcd for  $\text{C}_{16}\text{H}_{12}\text{O}_2\text{N}_3\text{Cl}$  313.0618 Found: 313.0615.

#### 6.2.3. 6-(4-Bromophenyl)amino-2,3-dimethyl-5,8-quinoxalinedione (**10c**)

Dark red powder (37%). mp: 255–257 °C.  $^1\text{H NMR}$  (DMSO- $d_6$ ):  $\delta$  9.4 (s, 1H, NH), 7.4–7.6 (m, 4H, benzene), 6.3 (s, 1H, H7), 2.6 (s, 6H, 2CH<sub>3</sub>). MS ( $m/z$ ): 357 ( $\text{M}^+$ ), 278, 222, 108, 96, 83, 55. HRMS ( $m/z$ ): Calcd for  $\text{C}_{16}\text{H}_{12}\text{O}_2\text{N}_3\text{Br}$  357.0110 Found: 357.0113.

#### 6.2.4. 2,3-Dimethyl-6-(4-ethoxyphenyl)amino-5,8-quinoxalinedione (**10d**)

Dark red needle (35%). mp: 217–219 °C.  $^1\text{H NMR}$  (DMSO- $d_6$ ):  $\delta$  9.3 (s, 1H, NH), 6.9–7.2 (m, 4H, benzene), 6.0 (s, 1H, H7), 4.1 (q, 2H,  $J = 7.2$ , CH<sub>2</sub>), 2.6 (s, 6H, 2CH<sub>3</sub>), 1.3 (t, 3H,  $J = 7.2$ , CH<sub>3</sub>). HRMS ( $m/z$ ): Calcd for  $\text{C}_{18}\text{H}_{17}\text{N}_3\text{O}_3$  323.1270 Found: 323.1295.

#### 6.2.5. 6-(3,5-Difluorophenyl)amino-2,3-dimethyl-5,8-quinoxalinedione (**10e**)

Dark red powder (31%). mp: 234–236 °C.  $^1\text{H NMR}$  (DMSO- $d_6$ ):  $\delta$  9.5 (s, 1H, NH), 7.16–7.18 (m, 1H, benzene), 7.03–7.08 (m, 2H, benzene), 6.4 (s, 1H, H7), 2.5 (s, 6H, 2CH<sub>3</sub>), HRMS ( $m/z$ ): Calcd for  $\text{C}_{16}\text{H}_{11}\text{F}_2\text{N}_3\text{O}_2$  315.0819 Found: 315.0814.

#### 6.2.6. 6-(3,4-Dichlorophenyl)amino-2,3-dimethyl-5,8-quinoxalinedione (**10f**)

Dark red powder (51%). mp: 213 °C (dec).  $^1\text{H NMR}$  (DMSO- $d_6$ ):  $\delta$  9.5 (s, 1H, NH), 7.68–7.69 (m, 2H, benzene), 7.42–7.45 (m, 2H, benzene), 6.2 (s, 1H, H7), 2.6 (s, 6H, 2CH<sub>3</sub>), HRMS ( $m/z$ ): Calcd for  $\text{C}_{16}\text{H}_{11}\text{Cl}_2\text{N}_3\text{O}_2$  347.0229 Found: 347.0225.

### 6.3. Molecular modeling

All computational studies were performed using Tripos SYBYL version 8.0.3 software package based on a Linux (RHEL 4.0 Intel Xeon processor 5050) workstation. The structures of the tested compounds were built with Concord and energy minimized using the Tripos force field and Gasteiger–Hückel charges (method: Powell, termination: gradient 0.05 kcal/mol Å, and max iterations: 1,000,000) implemented in the SYBYL.

### 6.3.1. Molecular alignment

Pharmacophore models of the representative molecules with high activities were generated using Genetic Algorithm with Linear Assignment of Hypermolecular Alignment of Database (GALAHAD) and a series of molecules was aligned to the selected pharmacophore model for 3D-QSAR studies.

### 6.3.2. 3D-QSAR studies using CoMFA and CoMSIA

The steric and electrostatic field energies for CoMFA were calculated using the SYBYL default parameters: 2.0 Å grid points spacing, an sp<sup>3</sup> carbon probe atom with +1 charge and a van der Waals radius of 1.52 Å, and column filtering of 2.0 kcal/mol. In CoMSIA, the steric, electrostatic, hydrophobic, hydrogen-bond donor and acceptor potential fields were calculated at each lattice intersection with the SYBYL default parameters and the attenuation factor of 0.3 was used.

The CoMFA and CoMSIA descriptors were used as independent variables, and pIC<sub>50</sub> values were used as dependent variables in partial least-squares (PLS) regression analyses to derive 3D-QSAR models. The optimum number of principal components is obtained by the leave-one-out (LOO) cross-validation procedure. Using the optimal number of principal components, the final PLS analyses were carried out to generate the predictive QSAR models without cross-validation process. To visualize the 3D-QSAR results in term of field contributions, isocontour maps were generated using the field type 'stdev \* coeff' and the contour levels were set to default values.

### Acknowledgments

This work was supported by the second stage of the Brain Korea 21 Project and grants from the Basic Research Program (R01-2006-000-10020-0) of the Korea Science and Engineering Foundation (KOSEF) to C.-K. Ryu and the National Core Research Center (NCRC) program (R15-2006-020) of the Ministry of Education, Science and Technology (MEST) and KOSEF through the Center for Cell Signaling & Drug Discovery Research at Ewha Womans University and the Ewha Womans University Research Grant of 2006 to S. Choi.

### References and notes

1. Ross, R. *Nature* **1993**, *362*, 801.
2. Middleton, R. W.; Parrick, J. In *The Chemistry of the Quinonoid Compounds*; Patai, S., Rappoport, Z., Eds.; John Wiley & Sons: London, 1988; pp 1019–1066. Part 2.
3. Hong, S.-Y.; Chung, K.-H.; You, H.-J.; Choi, I. H.; Chae, M. J.; Han, J.-Y.; Jung, O.-J.; Kang, S.-J.; Ryu, C.-K. *Bioorg. Med. Chem. Lett.* **2004**, *14*, 3563.
4. Chung, K.-H.; Hong, S.-Y.; You, H.-J.; Park, R.-E.; Ryu, C.-K. *Bioorg. Med. Chem.* **2006**, *14*, 5795.
5. Ryu, C.-K.; Lee, R.-Y.; Lee, S.-Y.; Chung, H.-J.; Lee, S. K.; Chung, K.-H. *Bioorg. Med. Chem. Lett.* **2008**, *18*, 2948.
6. Chung, H.-J.; Jung, O.-J.; Chae, M. J.; Hong, S.-Y.; Chung, K.-H.; Lee, S. K.; Ryu, C.-K. *Bioorg. Med. Chem. Lett.* **2005**, *15*, 3380.
7. Ryu, C.-K.; Song, E. H.; Shim, J.-Y.; You, H.-J.; Choi, K. U.; Choi, I. H.; Lee, E. Y.; Chae, M. J. *Bioorg. Med. Chem. Lett.* **2003**, *13*, 17.
8. Gum, W. F.; Joulie, M. M. *J. Org. Chem.* **1967**, *32*, 53.